New Template-Free Layered Manganese(III) Phosphate: Hydrothermal Synthesis, Ab Initio Structural Determination, and Magnetic Properties

Stanislav Ferdov,[†,‡,§] Armandina M. L. Lopes,[§,||] Zhi Lin,*[,†] and Rute A. Sá Ferreira[§]

Departments of Chemistry and Physics, CICECO, University of Aveiro, 3810-193 Aveiro, Portugal, and Department of Physics, IFIMUP, University of Porto, 4169-007 Porto, Portugal

Received July 20, 2007. Revised Manuscript Received September 25, 2007

A new template-free layered manganese(III) phosphate, $Na_3MnH(P_{0.9}O_4)_2$, has been hydrothermally synthesized. The crystal structure was solved ab initio from powder X-ray diffraction data, and the model was confirmed using the Rietveld method. The material crystallizes in triclinic space group $P\bar{1}$ (No. 2) with lattice parameters $a = 5.2925(2)$ Å, $b = 6.9004(3)$ Å, $c = 5.2452(3)$ Å, $\alpha = 91.56(0)°$, $\beta = 116.95(0)°$, $\gamma = 90.5(0)°$, and $Z = 1$. The structure consists of $[Mn(P_{0.9}O_4)_2]_\infty$ layers composed of isolated MnO_6 octahedra connected via corner-sharing asymmetric PO_4 tetrahedra. The interconnection between the layers is assured by Na^+ cations, which reside in the interlayered space. The system is paramagnetic above 50 K, with an effective paramagnetic moment of 4.85(3) μ_B, ascertaining the Mn^{3+} valence state of the Mn ions. Antiferromagnetic short-range-order effects are observed below 26.5 K.

1. Introduction

Manganese has one of the most varied oxidation states of all of the elements. Materials with Mn^{3+} or Mn^{4+} or both are widely used in batteries[1] and catalytic processes.[2–5] In this respect, manganese phosphates are used as catalysts for the oxidation of methyl mandelate[6] and of adonitol to ribose.[7] These materials also have useful coating characteristics and play a major role in the corrosion protection of mild steels[8] and as the intermediate layer before the final painting of automobile iron casting.[9] Finally, the electrochemical properties of manganese phosphates are now proving to be of industrial interest.[10,11]

Although manganese phosphates are among the most widespread of all mineral phosphates, the synthetic compounds with an open framework are very scarce and the chemistry of new phases in this area is emerging. The majority of the reported phases contain only Mn^{2+},[12,13] and open structures with Mn^{3+} are rare. One reason is the easy reduction of Mn^{3+} and/or Mn^{4+} materials to Mn^{2+} materials at high temperature. The other reason is the very low solubility of Mn^{3+} and Mn^{4+} in solution, which causes difficulties in the hydrothermal synthesis of open-structural materials with high crystallinity.[14] Furthermore, the majority of the open-framework manganese phosphates contain an organic molecule as a structure-forming unit.

In this paper, we report a new example of template-free layered manganese(III) phosphate, although 2-methylpentamethylenediamine (MPMD) has been used in its preparation. To date, MPMD is used only as a template for the preparation of crystalline mesoporous germanium oxides,[15] and here for the first time, we present the synthesis of a metal phosphate using MPMD. The present work also demonstrates a combination of laboratory powder X-ray diffraction (XRD) data, spectroscopic study, and magnetic properties for successful ab initio structural determination.

2. Experimental Section

2.1. Synthesis. A typical synthesis of $Na_3MnH(P_{0.9}O_4)_2$ is as follows. A solution of 0.47 g of NaH_2PO_4 (Aldrich) in 8.67 g of distilled water was mixed with 13.28 g of MPMD (Du Pont). Then, 0.05 g of $MnSO_4 \cdot H_2O$ (Aldrich) dissolved in 6.58 g of distilled water was added to the above solution. The resulting mixture was homogenized for 40 min and then transferred into a Teflon-lined

* Author to whom correspondence should be addressed. E-mail:zlin@ua.pt. Tel: 351 234401519. Fax: 351 234370084.
† Department of Chemistry, CICECO, University of Aveiro.
‡ On leave from the Central Laboratory of Mineralogy and Crystallography, Bulgarian Academy of Sciences.
§ Department of Physics, CICECO, University of Aveiro.
|| University of Porto.

(1) Chabre, Y.; Pannetier, J. *Prog. Solid State Chem.* **1995**, *23*, 1.
(2) Krishnan, V. V.; Suib, S. L. *J. Catal.* **1999**, *184*, 305.
(3) Wang, J.-Y.; Xia, G.; Yin, Y.-G.; Suib, S. L.; O'Young, C. L. O. *J. Catal.* **1998**, *176*, 321.
(4) Xia, G. G.; Yin, Y. G.; Willis, W. S.; Wang, J. Y.; Suib, S. L. *J. Catal.* **1999**, *185*, 91.
(5) Luo, J.; Zhang, Q.; Huang, A.; Suib, S. L. *Microporous Mesoporous Mater.* **2000**, *35–36*, 209.
(6) Malkani, R. K.; Suresh, K. S.; Bakore, G. V. *J. Indian Chem. Soc.* **1978**, *55* (3), 215.
(7) Fadnis, A. G.; Kulshrestha, S. K. *React. Kinet. Catal. Lett.* **1982**, *19* (3–4), 267.
(8) Talaat El-Mallah, A.; Hassib, A. M.; Farid, S. M. *Met. Finish.* **1988**, *86* (4), 29.
(9) Li, G.-Y.; Lian, J.-S.; Niu, L.-Y.; Jiang, Z.-H. *ISIJ Int.* **2005**, *45* (9), 1326.
(10) Takuaki, O.; Yoji, T.; Yoshio, U. *Jpn. Kokai Tokkyo Koho* **2006**, 13.
(11) Ojczyk, W.; Marzec, J.; Swierczek, K.; Molenda, J. *Diffus. Defect Data. Pt. A* **2005**, 237–240, 1299.
(12) Daidouh, A.; Martinez, J. L.; Pico, C.; Veiga, M. L. *J. Solid State Chem.* **1999**, *144*, 169.
(13) Escobal, J.; Mesa, J. L.; Pizarro, J. L.; Lezama, L.; Olazcuaga, R.; Rojo, T. *J. Mater. Chem.* **1999**, *9*, 2691.
(14) Tong, W.; Xia, G.-G.; Tian, Z.-R.; Liu, J.; Cai, J.; Suib, S. L.; Hanson, J. C. *Chem. Mater.* **2002**, *14* (2), 615.
(15) Zou, X.; Conradsson, T.; Klingstedt, M.; Dadachov, M. S.; O'Keeffe, M. *Nature* **2005**, *437*, 716.

10.1021/cm701951w CCC: $37.00
Published on Web 10/31/2007

autoclave (45 mL). The crystallization was performed under static conditions at 150 °C for 6 days. After fast cooling with flowing water, the run product was filtered with distilled water and dried at 40 °C for 1 day. The phase crystallizes as brownish 10–20 μm prismatic particles (see Figure S1 in the Supporting Information), whose shape facilitated the collection of a powder XRD pattern without preferential orientation. At present, $Na_3MnH(P_{0.9}O_4)_2$ must be prepared with MPMD in the starting mixture. However, this amine is not included in the crystal structure. Its presence in the starting mixture may only provide a proper initial condition for crystallization. In this respect, a future synthesis of $Na_3MnH(P_{0.9}O_4)_2$ using different chemical reactants could be possible.

The ion exchange was carried out by stirring 0.1 g of $Na_3MnH(P_{0.9}O_4)_2$ in a 1 M aqueous solution of CsCl. The reaction was performed at room temperature for 1 day. The ion-exchange product was collected by filtration, washed with distilled water, and dried in air for 1 day.

2.2. Characterization. The scanning electron microscopy images and chemical analysis (energy-dispersive spectrometry, EDS) were carried out using a scanning electron microscope, Hitachi S-4100, equipped with a Römteck EDS system. Powder XRD data were collected on a Philips X'pert MPD diffractometer (Cu $K\alpha_{1,2}$ X radiation) using a fixed divergence slit of 0.25°, and a flat-plate sample holder, in a Bragg–Brentano parafocusing optics configuration. The diffraction intensity was collected by the step scan method (step 0.01° and time 10 s) in the 2θ range between 7 and 77°. Fourier transform IR (FTIR) spectra of powdered samples suspended in KBr pallets were acquired between 400 and 4000 cm^{-1} using a Mattson 7000 spectrometer, with resolution 2 cm^{-1}. The thermogravimetry (TG) curve was collected with a Shimadzu TG-50 analyzer. The sample was heated in air at a rate of 5 °C min^{-1}. The photoluminescence spectra were recorded at room temperature with a modular double-grating excitation spectrofluorimeter with a TRIAX 320 emission monochromator (Fluorolog-3, Jobin Yvon-Spex) coupled to a R928 Hamamatsu photomultiplier, using the front-face acquisition mode. The excitation source was a 450 W xenon arc lamp. The emission spectra were corrected for detection and optical spectral response of the spectrofluorimeter, and the excitation spectra were corrected for the spectral distribution of the lamp intensity using a photodiode reference detector.

The magnetization measurements presented in this work were carried out using a commercial Quantum Design Superconducting Quantum Interference Device (SQUID) magnetometer (10^{-8} emu sensitivity). The direct current magnetic susceptibility was measured in a low magnetic field, $H = 49.6$ Oe, over the 5–290 K temperature range. The thermal dependence of magnetic susceptibility in the zero-field-cooling (ZFC) procedure was acquired after the sample had been cooled to 5 K with $H = 0$. After, the 49.6 Oe magnetic field was applied and the subsequent measurement was performed while increasing the temperature. In the field-cooling (FC) procedure, the sample was cooled down to the desired temperature under the 49.6 Oe applied field. The measurement was performed, with the same applied field, while increasing the temperature, as in the ZFC.

3. Results and Discussion

3.1. Structural Determination. The powder XRD peak positions and relative intensities were accurately determined by the software package *WinFit*.[16] The extracted information was included in the indexing programme *TREOR90*,[17] which indicated a triclinic unit cell. The same cell was confirmed by *DICVOL91*.[18] The choice of the space group in the estimated triclinic system cannot be made by examination of the systematic absences, and the selected centrosymmetric $P\bar{1}$ is based on a statistical study showing that there are more triclinic structures in $P\bar{1}$ than in $P1$. The ab initio crystal structure determination was carried out with the *EXPO* package.[19] First structure factor amplitudes were extracted by the Le Bail method.[20] The imperfect crystallinity of the compound led to peak broadening and, hence, very severe peak overlap. It was therefore necessary to try different angular limits for the pattern decomposition in order to obtain a sufficient number of meaningful intensities. Finally, the structure was solved by combining direct methods and difference Fourier synthesis. The atomic coordinates of the obtained structural model were refined using the *FullProf* programme.[21] The refinement was performed in the range 8–77° 2θ for 216 independent reflections involving the parameters shown in Table 1. The final Rietveld plot is shown in Figure 1, and the refined atomic coordinates are given in Table 2. Within experimental error, the EDS chemical analysis supports the Na/P/Mn (2.9:2.2:1.0) ratio obtained by powder XRD (3.0:1.8:1.0).

Table 1. Crystal Data and Structure Refinement Parameters

compound	$Na_3MnH(P_{0.9}O_4)_2$
chemical formula	$Na_3MnHP_{1.8}O_8$
fw (g mol^{-1})	308.656
cryst syst	triclinic
space group	$P\bar{1}$ (No. 2)
unit cell dimens	$a = 5.2925(2)$ Å, $b = 6.9004(3)$ Å, $c = 5.2452(3)$ Å, $\alpha = 91.56(0)°$, $\beta = 116.95(0)°$, $\gamma = 90.5(0)°$
V (Å^3)	170.64(17)
Z	1
D(calculated) (g/cm^3)	3.01(3)
wavelength	Cu $K\alpha_{1,2}$
2θ range (deg)	8.00–77.09
time per step (s)	10
2θ step size	0.01
no. of indep reflns	216
no. of profile refined param	13
no. of intensity-dependent refined param	26
zero point	0.145(5)
background polynomial param	+2207.9, −692.70, +599.16, −865.99, +464.90, −46.978
Caglioti law param (U, V, W)	+0.222(5), −0.1442(9), +0.094(9)
peak shape, η	pseudo-Voigt, 0.55(8)
reliability factors (conventional: background excluded) for points with Bragg contribution	$R_p = 12.4$, $R_{wp} = 10.3$, $R_{exp} = 6.31$, $\chi^2 = 2.81$
structure factors	$R_B = 4.11$, $R_F = 3.55$

Despite the relative simplicity of the crystal structure, no identical manganese phosphate has been found in the lit-

(16) Krumm, S. *Mater. Sci. Forum* **1996**, *228–231*, 183.

(17) Werner, P. E.; Eriksson, L.; Westdahl, M. *J. Appl. Crystallogr.* **1985**, *18*, 367.

(18) Boultif, A.; Louër., D. *J. Appl. Crystallogr.* **1991**, *24*, 987.

(19) Altamore, A.; Burla, M. C.; Cascarano, G.; Giacovazzo, C.; Guagliardi, A.; Moliterni, A. G. G.; Polidori, G. *J. Appl. Crystallogr.* **1995**, *28*, 842.

(20) Le Bail, A.; Duroy, H.; Fourquet, J. L. *Mater. Res. Bull.* **1988**, *23*, 447.

(21) Rodriguez-Carvajal, J. *Fullprof2k*, version 3.4; Laboratoire Leon Brillouin (CEA/CNRS), CEA-Saclay: Gif-sur-Yvette Cedex, France, Nov 2005.

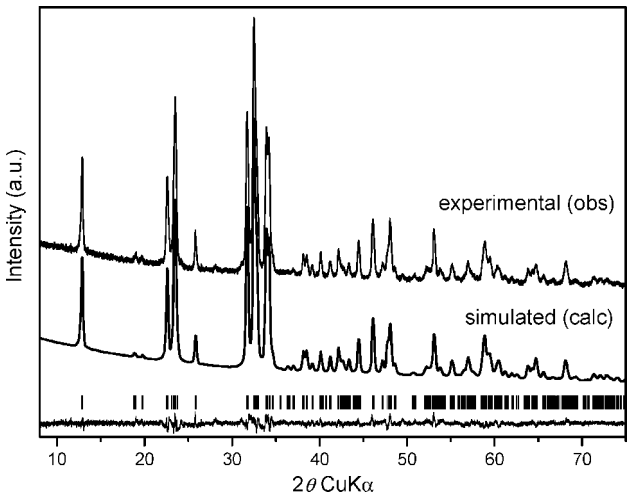

Figure 1. Experimental and simulated powder XRD patterns of $Na_3MnH(P_{0.9}O_4)_2$.

Table 2. Atomic Coordinates and Isotropic Displacement Parameters for $Na_3MnH(P_{0.9}O_4)_2$

atom	Wyckoff	SOF[a]	*x/a*	*y/b*	*z/c*	U_{iso} (Å^2)
Mn	1a	1	1	0	1	0.038(7)
P	2i	0.9	0.3568(9)	0.2494(5)	0.6529(8)	0.009(2)
Na1	1c	1	1	$^1/_2$	1	0.024(2)
Na2	2i	1	0.2954(9)	0.7818(5)	0.6657(9)	0.024(2)
O1	2i	1	0.6691(16)	0.2254(6)	0.7755(12)	0.036(7)
O2	2i	1	−0.2064(14)	0.7613(5)	0.6790(14)	0.036(7)
O3	2i	1	0.3034(10)	0.4612(9)	0.7521(13)	0.036(7)
O4	2i	1	0.2200(11)	0.0986(8)	0.7639(11)	0.036(7)

[a] SOF = site occupancy factor.

erature and Inorganic Crystal Structure Database. However, we came across a similar compound: $MgNa_3H(PO_4)_2$, where, instead of a trivalent transition element, a divalent alkaline-earth Mg cation is present.[22]

3.2. Structure Description. The structure of $Na_3MnH(P_{0.9}O_4)_2$ consists of anionic layers $[Mn(P_{0.9}O_4)_2]^{4-}$ stacked along the [010] direction. Each layer is built up from isolated MnO_6 octahedra sharing all of their corners with asymmetric PO_4 tetrahedra (Figure 2a). The charge of $[Mn(P_{0.9}O_4)_2]^{4-}$ is compensated for by two crystallographically independent Na^+ cations residing in the interlayer space (Figure 2b). The coordination of Na^+ cations is six (Na1) and eight (Na2), respectively. The Na1–O distance lies in the range of 2.410(8)−2.494(4) Å (average, 2.451 Å), while for Na2–O bonds, the distances vary in a broader range of 2.267(2)−3.013(8) Å (average, 2.617 Å). There is only one crystallographically distinct Mn cation forming a MnO_6 octahedron, which is characterized by two short apical Mn–O distances of 2.166(0) Å and four long equatorial ones of 2.211(6) and 2.269(6) Å (Table 3). This is interpreted as an "apically compressed" type of Jahn–Teller distortion, which points out a 3+ oxidation state of the Mn ions. As discussed later, this Mn oxidation state is confirmed by magnetization data analysis. The one unique P^{5+} cation is connected to four O atoms. Three of them are shared with those of the surrounding Mn octahedra and one points to the interlayer space. The lengths of the P–O bonds range from 1.490(0) to 1.608(0) Å

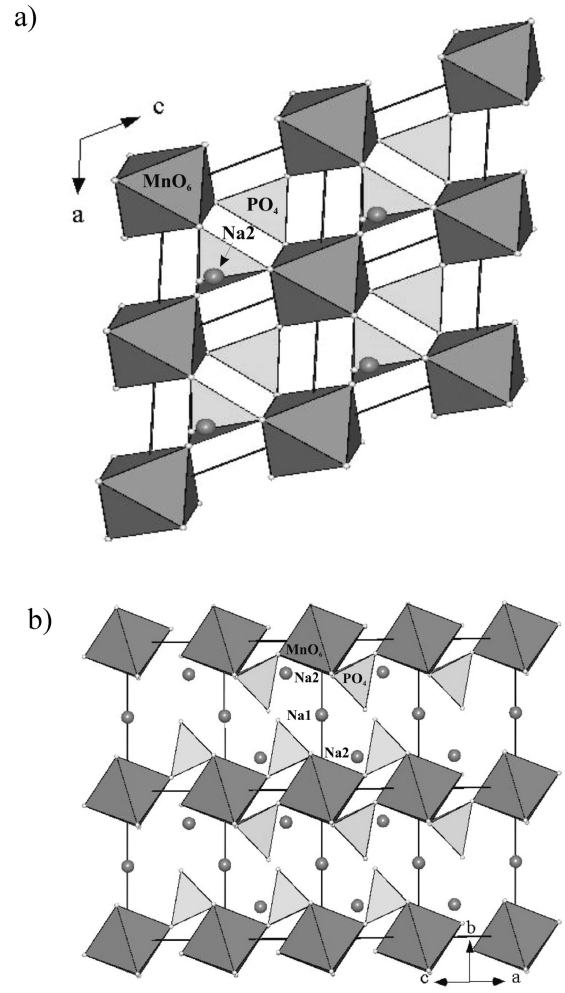

Figure 2. Structure of $Na_3MnH(P_{0.9}O_4)_2$ viewed along (a) [010] and (b) [101].

Table 3. Selected Bond Distances (Å) for $Na_3MnH(P_{0.9}O_4)_2$

Mn–O4	2x	2.166(0)	Na2–O3	1x	2.267(2)
Mn–O2	2x	>2.211(6)	Na2–O4	1x	2.311(6)
Mn–O1	2x	>2.269(6)	Na2–O1	1x	2.404(4)
P–O1	1x	>1.490(0)	Na2–O2	1x	2.611(0)
P–O4	1x	>1.532(3)	Na2–O2	1x	2.690(7)
P–O2	1x	>1.551(0)	Na2–O4	1x	2.787(2)
P–O3	1x	>1.608(0)	Na2–O1	1x	2.852(6)
Na1–O2	2x	>2.410(8)	Na2–O4	1x	3.013(8)
Na1–O1	2x	>2.448(5)			
Na1–O3	2x	>2.494(4)			

(average, 1.545 Å), indicating some degree of multiple-bond character. The longer distance of 1.608(0) Å observed in the terminal P–O3 bonds suggests the presence of a partial negative charge on the corresponding O atoms, which is consistent with the spectroscopically detected PO–H bonds (see IR spectroscopy). Considering the charge balance of the structure, the presence of H^+ increases the total positive charge. According to occupancy refinements, Mn and Na sites are fully occupied and no indication for lower electronic density on these positions has been detected. In contrast, the occupancy refinement of the P site gave a value of about 90%, and in this way, the resulting unoccupied tetrahedral positions compensate for the excess of positive charge. Details of the important bond distances and angles of $Na_3MnH(P_{0.9}O_4)_2$ are listed in Tables 3 and 4.

(22) Kawahara, A.; Yamakawa, J.; Yamada, T.; Kobashi, D. *Acta Crystallogr., Sect. C* **1995**, *51*, 2220.

Table 4. Selected Bond Angles (deg) for $Na_3MnH(P_{0.9}O_4)_2$

O1–P–O4	111.5(9)	O3–Na2–O4	150.2(9)
O1–P–O2	112.7(4)	O3–Na2–O1	101.2(1)
O1–P–O3	107.6(6)	O3–Na2–O2	90.2(8)
O2–P–O3	107.3(4)	O3–Na2–O2	83.1(1)
O4–P–O2	109.0(9)	O3–Na2–O4	113.8(8)
O4–P–O3	108.2(0)	O3–Na2–O1	76.2(9)
O4–Mn–O4	180.0(0)	O4–Na2–O1	107.8(4)
O4–Mn–O2	90.3(9)	O4–Na2–O2	109.1(6)
O4–Mn–O2	89.6(0)	O4–Na2–O2	76.3(5)
O4–Mn–O1	87.8(4)	O4–Na2–O4	70.6(1)
O4–Mn–O1	92.1(5)	O4–Na2–O1	75.6(4)
O2–Mn–O2	180.0(0)	O1–Na2–O2	60.4(8)
O2–Mn–O1	96.6(0)	O1–Na2–O2	122.2(7)
O2–Mn–O1	83.3(9)	O1–Na2–O4	72.2(9)
O1–Mn–O1	180.0(0)	O1–Na2–O1	172.2(7)
O2–Na1–O2	180.0(0)	O2–Na2–O2	173.2(2)
O2–Na1–O1	75.6(8)	O2–Na2–O4	130.4(3)
O2–Na1–O1	104.3(1)	O2–Na2–O1	111.9(9)
O2–Na1–O3	95.3(2)	O2–Na2–O4	54.5(4)
O2–Na1–O3	84.6(7)	O2–Na2–O1	64.9(8)
O2–Na1–O1	104.3(1)	O4–Na2–O1	115.4(2)
O1–Na1–O1	180.0(0)		
O1–Na1–O3	99.4(4)		
O1–Na1–O3	80.5(5)		
O1–Na1–O3	99.4(4)		
O3–Na1–O3	180.0(0)		

3.3. Spectroscopic Study. The FTIR transmittance spectrum of $Na_3MnH(P_{0.9}O_4)_2$ does not show the typical O–H bond stretching and H–O–H bond bending modes (Figure 3), confirming that there is no water and OH group in our sample. Furthermore, no vibration modes of amine were detected. According to the previous discussions by Britvin et al.[23] and Escobal et al.[24] on the IR spectra containing a PO–H group, the weak narrow bands at 2356 and 2166 cm^{-1} could correspond to the PO–H stretching vibrations,[23] and the bands observed at about 1350 and 1487 cm^{-1} can be assigned to the PO–H bending mode,[24] which is in a good agreement with the suggestion of the structural data. The asymmetric P–O stretching mode appears at 1042, 950, and 842 cm^{-1}, whereas the asymmetric O–P–O vibrations are observed at 552 and 485 cm^{-1}.[24,25]

In certain cases, photoluminescence is an efficient tool for the determination of the oxidation state of the Mn ions.[26] However, the collected spectra were not enough to give unambiguous evidence for the valence of the Mn ion, although a direct comparison between $Na_3MnH(P_{0.9}O_4)_2$ and compounds containing Mn^{2+} ($MnSO_4 \cdot 2H_2O$) and Mn^{3+} ($LaMnO_3$) was performed (see Figure S2 in the Supporting Information). The overlap of the emission spectra of the three phases suggested the necessity of using a complementary technique for unambiguous determination of the Mn oxidation state.

3.4. Ion Exchange. The layered structure of $Na_3MnH(P_{0.9}O_4)_2$ suggested that this material may be able to undergo an ion exchange, where the Na^+ cations are replaced by other cationic species. The performed chemical analysis on a number of different particles of the Cs-exchanged product gave the molar ratio Na:Cs:P:Mn = 0.3:1.0:0.6:1.0. Generally, in the layered compounds, the exchangeable cations are the ones residing in the interlayer. However, if we use Mn as a reference, both Na and P in the $Na_3MnH(P_{0.9}O_4)_2$ material were lost in ion exchange. Possible reasons for P loss could be the combination of two effects: partial occupation of the P site and the longer distance of the terminal P–O3 bond [1.608(0) Å], which makes it vulnerable (respectively PO_4 tetrahedra) toward changes in the interlayer composition. The powder XRD pattern of the Cs-exchanged product indicated an unknown phase whose structural determination is in progress.

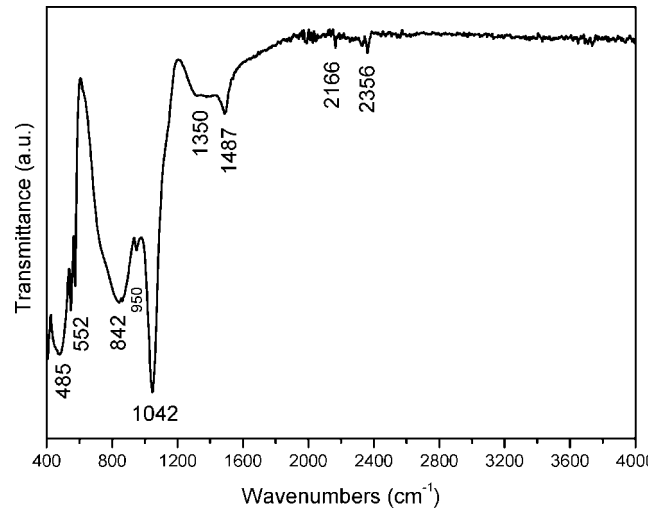

Figure 3. FTIR spectrum of $Na_3MnH(P_{0.9}O_4)_2$.

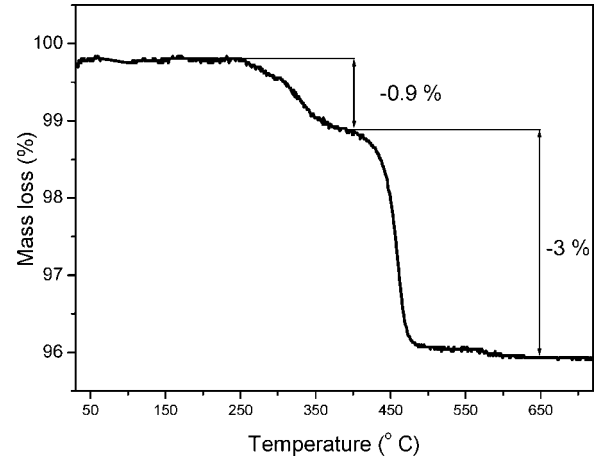

Figure 4. TG curve of $Na_3MnH(P_{0.9}O_4)_2$.

3.5. Thermal Behavior. The TG curve of $Na_3MnH(P_{0.9}O_4)_2$ is composed of two main steps showing a total mass loss of 3.9% up to about 650 °C (Figure 4). The first step corresponds to 0.9% (between 250 and 400 °C) mass loss and the second one to 3.0% (between 400 and 650 °C) mass loss. These two steps can be attributed to the thermal decomposition of $Na_3MnH(P_{0.9}O_4)_2$ and subsequent phase transformation.[27] The run product of the thermal analysis was studied by powder XRD, which indicated a mixture of

(23) Britvin, S. N.; Ferraris, G.; Ivaldi, G.; Bogdanova, A.; Chukanov, N. V. *N. Jb. Miner. Mh.* **2002**, *4*, 160.
(24) Escobal, J.; Pizarro, J. L.; Mesa, J. L.; Lezama, L.; Olazcuaga, R.; Arriortua, M. I.; Rojo, T. *Chem. Mater.* **2000**, *12*, 376.
(25) Fernandez, S.; Mesa, J. L.; Pizarro, J. L.; Lezama, L.; Arriortua, M. I.; Olazcuaga, R.; Rojo, T. *Chem. Mater.* **2000**, *12*, 2092.
(26) Solé, J. G.; Bausá, L. E.; Jaque, D. *An Introduction to the Optical Spectroscopy of Inorganic Solids*; John Wiley & Sons Ltd.: New York, 2005; p 211.
(27) Macintyre, J. E., Daniel, F. M., Stirling, V. M., Eds. *Dictionary of Inorganic Compounds*; Chapman & Hall:London,1992.

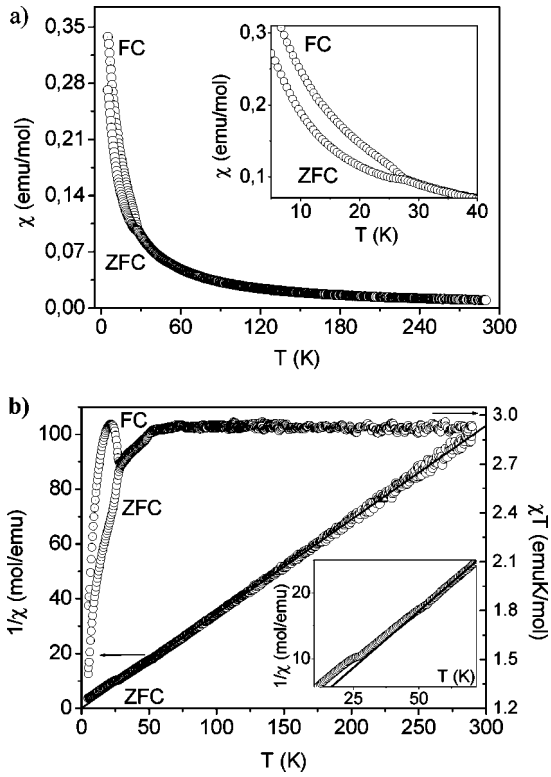

Figure 5. ZFC and FC magnetization measurements for the $Na_3MnH(P_{0.9}O_4)_2$ compound: (a) Thermal evolution of the molar susceptibility, χ. Inset: detail on the 0–40 K temperature range. (b) ZFC $1/\chi$ vs T curve and the corresponding linear fit according the Curie–Weiss law (left scale); thermal evolution of χT (right scale). Inset: detail on the ZFC $1/\chi$ vs T curve for the 10–72 K temperature range.

Na_3PO_4 (PDF No. 84-0196) and unknown phases (see Figure S3 in the Supporting Information). This fact supports the suggestion for thermal evolution. However, the mixed-phase product has prevented us from an estimation of the exact decomposition path.

3.6. Magnetic Properties. The magnetic susceptibilities of ZFC and FC curves of $Na_3MnH(P_{0.9}O_4)_2$ are shown in Figure 5. The presented curves were corrected from the temperature-independent paramagnetism, χ_0, estimated from the fit of the linearized plot, χ vs $1/T$, for $T \gg \theta$ (in the paramagnetic region for $T \gg \theta$, the Curie–Weiss law can be written as $\chi \approx \chi_0 + C/T$, where C is the Curie constant and θ is the Curie–Weiss temperature).

As one can observe in Figure 5a, the molar susceptibility shows a monotonic increase with decreasing temperature down to 26.5 K, where inflection is observed. This effect can be associated with a short-range order between the Mn ions;[28] its nature will be discussed later. In Figure 5b, the $1/\chi$ vs T curve is presented. At temperatures above 50 K, the paramagnetic behavior of the Mn spins is evident. The paramagnetic data were fitted to the Curie–Weiss equation, $\chi = C/(T - \theta)$, yielding a Curie constant $C = 2.94(2)$ emu K mol^{-1}. From this value, an effective magnetic moment of 4.85(3) μ_B is obtained for the Mn ions. This value is in excellent agreement with the spin-only Mn^{3+} value, 4.90 μ_B. The Curie–Weiss temperature was found to be $\theta = -0.8(5)$ K. These results, together with the constant value observed in the χT curve above 50 K, give strong evidence for paramagnetic behavior of this compound. Consequently, it points out the presence of isolated magnetic ions. This is in conformity with the crystallographic structure, where no Mn–O–Mn bonds exist and the possible exchange pathways are the Mn–O–P–O–Mn, where the O–P–O bond angles, far from 180° (see the structure description), favor small exchange integrals, justifying the weak interactions observed.[28]

For temperatures below 50 K, a deviation from the Curie–Weiss law is observed (see $1/\chi$ vs T curve) for both the ZFC and FC curves. In addition, the χT curves decrease continuously with decreasing temperature, suggesting the onset of antiferromagnetic correlations. Below 26.5 K, a clear dependence on the cooling conditions is observed, hinting for antiferromagnetic short-range order effects and/or magnetic frustration due to the competition between dipolar and the small exchange magnetic interactions. To obtain further insight on the observed short-range order effects, a detailed magnetic study is in progress.

4. Conclusion

A new, rare example of layered sodium manganese(III) phosphate is synthesized by a hydrothermal method using, for the first time, MPMD. The crystal structure is solved ab initio from powder XRD data. This compound differs from the majority of synthetic manganese phosphates in that the Mn ion is presented in oxidation state 3+. Furthermore, the treatment of $Na_3MnH(P_{0.9}O_4)_2$ by an aqueous solution of CsCl results in the formation of a new Cs-containing phase whose structural determination is in progress. Measured magnetic properties show that the material is paramagnetic above 50 K, with an effective paramagnetic moment of 4.85(3) μ_B, ascertaining the valence of Mn^{3+}. Antiferromagnetic short-range order sets in below 26.5 K. A further work on the details of the short-range order is in progress.

Acknowledgment. The authors gratefully thank J. P. Araújo and V. S. Amaral for fruitful discussions. The authors are thankful for financial support from FCT, POCI2010, and FEDER. S.F. and A.M.L.L. also thank FCT (Grant SFRH/BPD/23771/2005) and (Grant SFRH/BPD/32778/2005) for the grants.

Note Added after ASAP Publication. This paper published ASAP on October 31, 2007 with an error in the Magnetic Properties section; the corrected version published ASAP November 2, 2007.

Supporting Information Available: Figures S1–S3. This material is available free of charge via the Internet at http://pubs.acs.org.

CM701951W

(28) Song, Y.; Zavalij, P. Y.; Suzuki, M.; Whittingham, M. S. *Inorg. Chem.* **2002**, *41*, 5778.